JOURNAL OF SPACECRAFT AND ROCKETS
Vol. 43, No. 3, May–June 2006

Equilibrium-to-Equilibrium Maneuvers of Flexible Electrodynamic Tethers in Equatorial Orbits

Kalyan K. Mankala* and Sunil K. Agrawal†
University of Delaware, Newark, Delaware 19716

The relative equilibria for satellite tether systems, when the tether is modeled as a single rigid pendulum, have been characterized. The satellite, to which the tether is attached, was assumed to move in equatorial circular orbits. The magnetic field of the Earth was modeled as a nontilted dipole. In the presence of electrodynamic forces, a control resistor in series with the tether resistance was used for equilibrium-to-equilibrium maneuvers of the tether. This idea is extended to study relative equilibria of flexible, but massless, tethers. The effects of electrodynamic forces on the tether are considered. The relative equilibrium configurations of the system are studied assuming that one of the satellites is very massive, that is, it is constrained to a certain orbit and it is not affected by the motion of the tether and the end mass. The relative equilibrium configurations are found to be unstable. A control resistor in series with the electrodynamic tether is used to regulate the tether around its equilibrium configurations. The control resistor is also used to perform equilibrium-to-equilibrium maneuvers of this underactuated system.

Nomenclature

$\boldsymbol{B}$	=	magnetic field intensity at the orbital location
$\mathcal{E}$	=	voltage/emf developed across the tether
$\hat{\boldsymbol{e}}_r$–$\hat{\boldsymbol{e}}_\theta$	=	orbital frame
I	=	current flowing through the tether
L	=	total unstretched arc length of the tether
M	=	mass of the Earth
m_A	=	mass of subsatellite $\mathcal{A}$
$\boldsymbol{p}_A$	=	position vector of $\mathcal{A}$ with respect to the origin of the inertial frame
$\boldsymbol{p}_{AB}, \boldsymbol{r}_A$	=	position vector of $\mathcal{A}$ with respect to $\mathcal{B}$
$\boldsymbol{p}_B$	=	position vector of $\mathcal{B}$ with respect to the origin of the inertial frame, $p_B = R_0$
R_A	=	distance of $\mathcal{A}$ from the center of Earth
Res_i	=	inherent resistance of the tether
Res_u	=	control resistance
$\boldsymbol{r}$	=	position vector of a tether element located at $\bar{s}$ with respect to $\mathcal{B}$
$\bar{s}$	=	unstretched arc length of the tether measured from $\mathcal{B}$
$\boldsymbol{X}$–$\boldsymbol{Y}$	=	inertial frame
ω	=	angular velocity of $\mathcal{B}$

I. Introduction

A CONDUCTIVE tether rotating in Earth's magnetic field generates a potential across the tether. When plasma guns are used, an electric current can be generated in the tether. The Tethered Satellite System Reflight (TSS-1R) mission has successfully demonstrated this idea. The current generated in the tether interacts with the magnetic field of the Earth to produce electrodynamic force. This electrodynamic force has applications in deorbiting and reboosting of a satellite.[1–4] Gravity gradient stabilizes a nonconducting tether to a radial equilibrium configuration. On the other hand, electrodynamic forces present in a conducting tether change the equilibrium configuration of the tether away from the radial configuration. Forward et al.[1] discuss the optimization of the tether angle, for a rigid tether model, to maximize the electrodynamic force in the tangential direction in the stable equilibrium configuration. Guidance and control strategies are required to achieve these optimum tether configurations and to maneuver the tether from one configuration to another. This is a requirement in momentum transfer missions[5] that involve rendezvous of tether end with a target. Mankala et al.,[6] dealt with these issues for a rigid-tether model using a control resistor in series with the inherent tether resistance. The objective of this paper is to extend these control ideas to a flexible and massless tethered system.

In the rigid-tether model considered by Mankala et al.,[6] under the assumption of planar equatorial circular orbit and nontilted dipole magnetic field, it is shown that the tethered system characterized by single degree of freedom has stable equilibrium configurations. A variable resistor in series with the tether resistance was used as an actuator to perform equilibrium-to-equilibrium maneuvers.

In this paper, we consider a flexible massless tethered system. We assume that the satellite containing the flexible tether is massive compared to the subsatellite at the other end of the tether. Because of this assumption, the motion of the primary satellite is assumed to stay in a circular equatorial orbit and is considered to be unaffected by the dynamics of the subsatellite. The magnetic field of the Earth is modeled by a nontilted magnetic dipole. Beletsky and Levin[7] have shown that the system under consideration has unstable equilibrium configurations. This is done by looking at the characteristic equation of linearized in-plane oscillations about an equilibrium configuration. The Routh–Hurwitz condition suggests that the charateristic equation has eigenvalues with positive real parts. In this paper, we develop control strategies to stabilize the system around these equilibrium configurations and perform equilibrium-to-equilibrium maneuvers. We show that the planar massless flexible system is a two-degree-of-freedom system, with a single control input, that is, an underactuated system.

In the literature, both linear and nonlinear current–voltage, I–$\mathcal{E}$, characteristics are used, while modeling an electrodynamic tether. Forward et al.,[1] Corsi and Iess[8] use the linear I–$\mathcal{E}$ characteristics to study deorbiting using an electrodynamic tether. Pelaez et al.[9] and Dobrowolny[10] use a nonlinear I–$\mathcal{E}$ model to study the dynamic instabilities in an electrodynamic tether. Because the main aim of this paper is to study the use of a variable resistor as an actuator, we have chosen to use a linear I–$\mathcal{E}$ model. We believe that this study will provide an insight into using the control resistor for nonlinear I–$\mathcal{E}$ models.

In summary, the primary contribution of the paper is to use the variable resistor in series with the tether resistance as a control

Presented as Paper 2004-5342 at the AIAA Guidance, Navigation, and Control Conference, Providence, RI, 16–19 August 2004; received 15 October 2004; revision received 7 June 2005; accepted for publication 13 July 2005.

*Graduate Student, Department of Mechanical Engineering; mankala@me.udel.edu. Student Member AIAA.

†Professor, Department of Mechanical Engineering; agrawal@me.udel.edu.

variable to regulate the unstable equilibrium configurations and to perform equilibrium-to-equilibrium maneuvers. Resistance of the control resistor can be changed by using a simple potentiometer actuated by a small motor. On the contrary, the subsatellite can also be moved to different equilibria by using thrusters onboard the subsatellite. The fuel needed by these thrusters acts as additional payload mass and may increase the cost of placing the main shuttle (satellite) hosting the tether system into a particular orbit. Also, the energy required to run a small motor is quite less compared to the energy required by the thrusters to move the subsatellite. Hence, we believe that the method of changing the resistance is more energy efficient than applying thrust forces to the subsatellite for stabilization and equilibrium-to-equilibrium maneuvers of the tether. Moreover, when the tether is modeled as a varying length flexible body with mass, a boundary control in the form of torque input[11] leaves the system highly underactuated. In these situations, a variable resistor, in addition to the torque input, can be used for improving the controllability of the system.

The rest of the paper is organized as follows: In Sec. II, the massless flexible tether model is described and the governing dynamics of the system are derived. Section III describes the relative equilibrium configurations of this system. Stabilization of the tether around equilibrium configurations using linearized models is dealt with in Sec. IV. In Sec. V, a nonlinear control based on feedback linearization of the dynamics is introduced.

II. Model and Equations of Motion

Figure 1 shows the model of a flexible tether system. Point mass $\mathcal{B}$ is the main satellite rotating around the Earth in an equatorial circular orbit. Point mass $\mathcal{A}$ is the subsatellite connected to $\mathcal{B}$ through a massless flexible tether. We assume that the whole system is restricted to the orbital plane and the satellite $\mathcal{B}$ is restricted to circular equatorial orbits of radius R_0. The latter condition is equivalent to assuming that the mass of satellite $\mathcal{A}$ is considerably small compared to that of satellite $\mathcal{B}$ or that thruster impacts keep $\mathcal{B}$ in its prescribed orbit. The magnetic field of the Earth is modeled by a nontilted magnetic dipole. The strength of the magnetic field and the ion density are generally significant in low Earth orbits alone. In these orbits, the velocity of the magnetic field due to the rotation of the Earth is considered to be less important compared to the velocity of the satellite. Hence, is not considered in the calculation of the electric potential developed across the tether.

A. Equation of Motion of Tether

In Fig. 1, $\hat{\boldsymbol{e}}_r$ and $\hat{\boldsymbol{e}}_\theta$ axes describe the rotation of the main shuttle $\mathcal{B}$ around the Earth with respect to an inertial X–Y frame. The position of the subsatellite is described in x–y frame that coincides with the orbital $\hat{\boldsymbol{e}}_r$–$\hat{\boldsymbol{e}}_\theta$ frame. This is shown in Fig. 1. In this paper, we use $\hat{\boldsymbol{e}}_r$–$\hat{\boldsymbol{e}}_\theta$ axes interchangeably with x–y axes because they coincide.

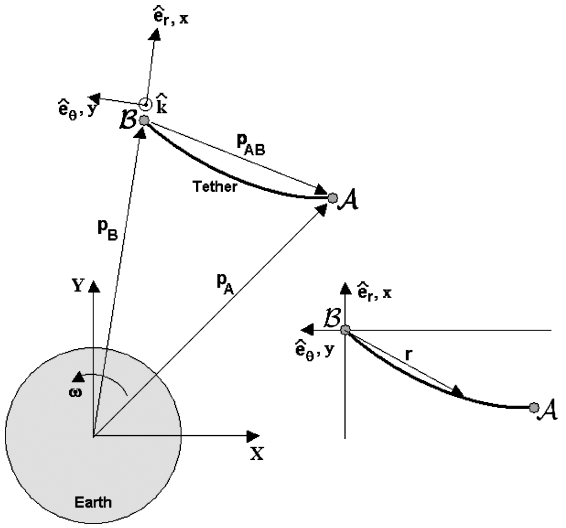

Fig. 1 Massless flexible tether system connecting two point mass satellites.

Let $\boldsymbol{n}$ indicate the tension in the tether at a location $\bar{s}$ from $\mathcal{B}$. Let $\mathrm{d}\boldsymbol{F}$ be the electrodynamic force acting on the small tether element located at $\bar{s}$. For this small tether element, we have

$$\boldsymbol{n}(\bar{s}+\mathrm{d}\bar{s})-\boldsymbol{n}(\bar{s})+\mathrm{d}\boldsymbol{F}=0 \tag{1}$$

In Eq. (1), gravity and inertia terms are absent because the tether is considered to be massless. Let $\boldsymbol{r}$ be the position vector of an element at a distance $\bar{s}$ from $\mathcal{B}$. Then the tension in the tether can be derived from the constitutive equations as

$$\boldsymbol{n}=EA(\|\boldsymbol{r}'\|-1)(\boldsymbol{r}'/\|\boldsymbol{r}'\|) \tag{2}$$

where $\boldsymbol{r}'$ indicates derivative of $\boldsymbol{r}$ with respect to $\bar{s}$, E is the Young's modulus of the tether material, A is the area of cross section of the tether. For more details please refer to Mankala and Agrawal.[11] The electrodynamic force [Lorentz force (see Ref. 12)] $\mathrm{d}\boldsymbol{F}$ can be related to the current I flowing through the tether in the following way:

$$\begin{aligned}\mathrm{d}\boldsymbol{F} &= I\,\mathrm{d}\boldsymbol{l}\times\boldsymbol{B}\\ &= I\,\mathrm{d}\bar{s}\,\boldsymbol{r}'\times\boldsymbol{B}\end{aligned} \tag{3}$$

From Eqs. (1–3), we have

$$\frac{\mathrm{d}\boldsymbol{n}}{\mathrm{d}\bar{s}}+\frac{\mathrm{d}\boldsymbol{F}}{\mathrm{d}\bar{s}}=0\Rightarrow\frac{\mathrm{d}}{\mathrm{d}\bar{s}}\left[EA(\|\boldsymbol{r}'\|-1)\frac{\boldsymbol{r}'}{\|\boldsymbol{r}'\|}\right]+I\boldsymbol{r}'\times\boldsymbol{B}=0 \tag{4}$$

B. Tether Configurations

Because Eq. (4) is a static equation, simplifying it gives an idea of the local shape of the tether. Expanding the first term in Eq. (4), we get

$$\begin{aligned}&\frac{\mathrm{d}}{\mathrm{d}\bar{s}}[EA(\|\boldsymbol{r}'\|-1)]\frac{\boldsymbol{r}'}{\|\boldsymbol{r}'\|}+EA(\|\boldsymbol{r}'\|-1)\frac{\mathrm{d}}{\mathrm{d}\bar{s}}\frac{\boldsymbol{r}'}{\|\boldsymbol{r}'\|}\\ &\quad+I\boldsymbol{r}'\times\boldsymbol{B}=0\end{aligned} \tag{5}$$

We know that $\boldsymbol{r}'$ is perpendicular to $(\boldsymbol{r}'\times\boldsymbol{B})$ and $(\mathrm{d}/\mathrm{d}\bar{s})(\boldsymbol{r}'/\|\boldsymbol{r}'\|)$ is perpendicular to $\boldsymbol{r}'$. Proof of the latter is shown next. Mathematically, let

$$\boldsymbol{\tau}=\frac{\boldsymbol{r}'}{\|\boldsymbol{r}'\|}\Rightarrow\boldsymbol{\tau}\cdot\boldsymbol{\tau}=1\Rightarrow\frac{\mathrm{d}\boldsymbol{\tau}}{\mathrm{d}\bar{s}}\cdot\boldsymbol{\tau}=0\Rightarrow\frac{\mathrm{d}}{\mathrm{d}\bar{s}}\left[\frac{\boldsymbol{r}'}{\|\boldsymbol{r}'\|}\right]\cdot\boldsymbol{r}'=0 \tag{6}$$

Equation (5) can be decomposed into the directions of $\boldsymbol{r}'$ and perpendicular to $\boldsymbol{r}'$ as follows:

$$\frac{\mathrm{d}}{\mathrm{d}\bar{s}}[EA(\|\boldsymbol{r}'\|-1)]\frac{\boldsymbol{r}'}{\|\boldsymbol{r}'\|}=0\Rightarrow EA(\|\boldsymbol{r}'\|-1)=\mathrm{const}=T \tag{7}$$

$$EA(\|\boldsymbol{r}'\|-1)\frac{\mathrm{d}}{\mathrm{d}\bar{s}}\frac{\boldsymbol{r}'}{\|\boldsymbol{r}'\|}+I\boldsymbol{r}'\times\boldsymbol{B}=0 \tag{8}$$

Equation (7) suggests that the magnitude of the tension at any point in the tether is constant. Based on this result, Eq. (8) gives an idea of the local shape of the tether. First, consider the derivative of the tangent vector $\boldsymbol{\tau}$ with respect to the stretched arc length s of the tether:

$$\frac{\mathrm{d}\boldsymbol{\tau}}{\mathrm{d}s}=\rho_t\hat{\boldsymbol{\tau}}_\perp=\frac{1}{R_t}\hat{\boldsymbol{\tau}}_\perp \tag{9}$$

where ρ_t is the curvature and R_t is the radius of curvature. For the unstretched arc length $\bar{s}$, we get

$$\begin{aligned}\frac{\mathrm{d}\boldsymbol{\tau}}{\mathrm{d}\bar{s}} &= \frac{\mathrm{d}\boldsymbol{\tau}}{\mathrm{d}s}\frac{\mathrm{d}s}{\mathrm{d}\bar{s}}\\ &= \frac{1}{R_t}\hat{\boldsymbol{\tau}}_\perp\|\boldsymbol{r}'\|\end{aligned} \tag{10}$$

Substituting Eq. (10) in Eq. (8) gives

$$R_t=EA(\|\boldsymbol{r}'\|-1)/|I|B_0=T/|I|B_0 \tag{11}$$

$$\hat{\boldsymbol{\tau}}_\perp=-[(\boldsymbol{r}'\times\boldsymbol{B})/\|\boldsymbol{r}'\times\boldsymbol{B}\|]\mathrm{sgn}(I) \tag{12}$$

where $B_0 = \|\boldsymbol{B}\|$. Note that $\|\boldsymbol{r}' \times \boldsymbol{B}\| = \|\boldsymbol{r}'\|\|\boldsymbol{B}\|$. Equation (11) suggests that the radius of curvature at any part of the tether is a constant. Consequently, the tether takes the shape of an arc of a circle during the entire motion. Convexity or concavity of the arc is decided by the the sign of the current. S-shaped curves, two arcs of same radius of curvature but with different curvature directions, have an inflection point at the intersection of the two arcs. Such S-shaped configurations are not possible for the electrodynamic tether. The curvature $\rho_t = 1/R_t = |I|B_0/T$ can be zero only if $I = 0$ and/or $\|\boldsymbol{r}'\| = \infty$. If $I = 0$, the tether takes the shape of a straight line. Please note that for a bare electrodynamic tether, current collection is done over a certain length of the tether. The current collection soon gets saturated and then remains constant over the rest of the tether length. To comment on the convexity or concavity of the tether in different quadrants of the orbital frame, the current expression is needed.

C. Current Through the Tether *I*

We assume a linear relation between current collection and the voltage developed across the tether, that is, $I = \mathcal{E}/\text{Res}$. In the following we decompose a vector from $\mathcal{B}$ to a point on the tether in the orbital frame as $\boldsymbol{r} = x\hat{\boldsymbol{e}}_r + y\hat{\boldsymbol{e}}_\theta$. If $\boldsymbol{V}_{\mathrm{d}\bar{s}}$ represents the velocity of the tether element in the inertial frame, using Faraday's law of induction,[12] the electric potential $\mathcal{E}$ developed across the tether can be derived to be

$$\mathcal{E} = \int_0^L \boldsymbol{V}_{\mathrm{d}\bar{s}} \times \boldsymbol{B} \cdot \mathrm{d}\boldsymbol{r}$$

$$\Rightarrow I = \frac{\mathcal{E}}{\text{Res}} = \frac{1}{\text{Res}} \int_0^L [\dot{\boldsymbol{p}_B} + \dot{\boldsymbol{r}}] \times B_0 \hat{\boldsymbol{k}} \cdot \boldsymbol{r}' \, \mathrm{d}\bar{s}$$

$$= \frac{B_0}{\text{Res}} \left[\omega \boldsymbol{p}_B \cdot \boldsymbol{p}_{AB} + \frac{1}{2}\omega {\boldsymbol{p}_{AB}}^2 + \int_0^L (x'\dot{y} - \dot{x}y') \, \mathrm{d}\bar{s} \right] \tag{13}$$

In Eq. (13), the first term in the brackets dominates because $\boldsymbol{p}_B$ is the orbit radius. We can approximate the current in the tether with the first term or the first two terms as

$$I \approx (B_0/\text{Res})\left(\omega \boldsymbol{p}_B \cdot \boldsymbol{p}_{AB} + \tfrac{1}{2}\omega {\boldsymbol{p}_{AB}}^2\right) \tag{14}$$

The sign of the current is predominantly dictated by x_A because $\boldsymbol{p}_B \cdot \boldsymbol{p}_{AB} = R_0 x_A$. If $x_A > 0$, then $I > 0$ and vice versa. This will determine the direction of the curvature of the arc from Eq. (12). Figure 2a shows the curvature of the tether in different quadrants of the orbital frame. Note that Res in the Eq. (14) can be thought of as a control resistor Res_u in series with the inherent tether resistance Res_i, that is, $\text{Res} = \text{Res}_u + \text{Res}_i$.

So far, we have shown that 1) the tether always takes the shape of an arc of a circle and 2) the tension in the tether is constant. These results are valid at equilibrium as well as during transient motion.

D. Equation of Motion of Body $\mathcal{A}$

Forces acting on $\mathcal{A}$ are 1) the gravitational force, 2) tension force $-\boldsymbol{n}(L)$, and 3) the inertia force. Using Newton's laws, we have

$$-\left(GMm_A \big/ \|\boldsymbol{p}_A\|^2\right)(\boldsymbol{p}_A/\|\boldsymbol{p}_A\|) - \boldsymbol{n}(L) = m_A \ddot{\boldsymbol{p}}_A \tag{15}$$

Note that we can write, using Fig. 1,

$$\begin{aligned} \boldsymbol{p}_A &= \boldsymbol{p}_B + \boldsymbol{p}_{AB} \\ &= R_0 \hat{\boldsymbol{e}}_r + \boldsymbol{p}_{AB} \\ &= R_0 \hat{\boldsymbol{e}}_r + \boldsymbol{r}_A \end{aligned} \tag{16}$$

From Fig. 2b, we can see that $\boldsymbol{n}(L)$ is along the direction of the unit vector $\hat{\boldsymbol{u}}$, at an angle α to the position vector $\boldsymbol{p}_{AB} (= \boldsymbol{r}_A)$. $\boldsymbol{p}_{AB_\perp}$ denotes a vector perpendicular to $\boldsymbol{p}_{AB}$ and in the direction of inward normal to the circular arc. Using this notation, we have

$$\boldsymbol{n}(L) = EA(\|\boldsymbol{r}'\| - 1)\hat{\boldsymbol{u}} \tag{17}$$

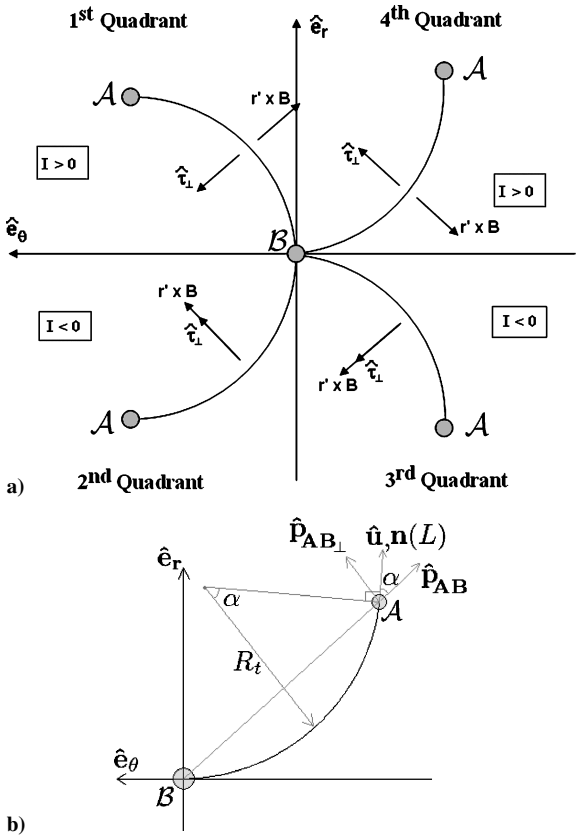

Fig. 2 Tether configuration: a) sign of the current and curvature direction and b) massless tether model with additional symbols.

where

$$\hat{\boldsymbol{u}} = \cos(\alpha)\hat{\boldsymbol{p}}_{AB} + \sin(\alpha)\hat{\boldsymbol{p}}_{AB_\perp} \tag{18}$$

$$\hat{\boldsymbol{p}}_{AB_\perp} = -\text{sgn}(I)\hat{\boldsymbol{p}}_{AB} \times \hat{\boldsymbol{k}} \tag{19}$$

If L^* is the stretched length of the tether, then from the geometry in Fig. 2b, we have $R_t(2\alpha) = L^*$. Because $L^* = \|\boldsymbol{r}'\|L$, we get

$$\alpha = \|\boldsymbol{r}'\|L/2R_t \tag{20}$$

From the geometry, we have $p_{AB} = 2R_t \sin(\alpha)$, that is,

$$p_{AB} = 2R_t \sin(\|\boldsymbol{r}'\|L/2R_t) \tag{21}$$

In summary, the tension in the tether, T, radius of curvature of the tether, R_t, and the current through the tether, I, are all implicitly given by the subsatellite position $\boldsymbol{p}_{AB}$ through the Eqs. (11), (14), and (21). The dynamics of the subsatellite is given by Eq. (15). Essentially it is a two-degree-of-freedom system, parameterized by the vector $\boldsymbol{p}_{AB}$, or by its coordinates along the orbital frame, x_A and y_A.

III. Relative Equilibrium Configurations

Relative equilibrium configurations denote the tether configurations that are stationary in orbital frame. The relative equilibrium configurations of the system can be determined from the body $\mathcal{A}$ dynamic Eq. (15) by making the rates in the orbital frame to be zero. Doing so, we get

$$-\left(GMm_A \big/ \|\boldsymbol{r}_A\|^2\right)(\boldsymbol{p}_A/\|\boldsymbol{p}_A\|) - EA(\|\boldsymbol{r}'\| - 1)\hat{\boldsymbol{u}} = -m_A\omega^2 \boldsymbol{p}_A \tag{22}$$

where

$$|I| = \frac{EA(\|\boldsymbol{r}'\| - 1)}{B_0 R_t} = \left| \frac{B_0\omega}{\text{Res}} \left[R_0 x_A + \frac{\left(x_A^2 + y_A^2\right)}{2} \right] \right| \tag{23}$$

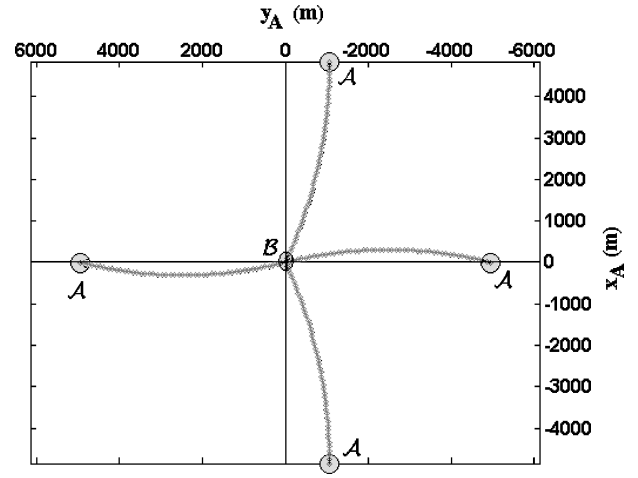

Fig. 3 Equilibrium configurations when $m_A = 100$ kg and $\text{Res}_u = 50\ \Omega$.

$$p_{AB} = 2R_t \sin\left(\frac{\|\boldsymbol{r}'\|L}{2R_t}\right) \tag{24}$$

$$\hat{\boldsymbol{u}} = \cos(\alpha)\hat{\boldsymbol{p}}_{AB} + \sin(\alpha)\hat{\boldsymbol{p}}_{AB_\perp} \tag{25}$$

$$\alpha = \frac{L^*}{2R_t} = \frac{\|\boldsymbol{r}'\|L}{2R_t} \tag{26}$$

$$\hat{\boldsymbol{p}}_{AB_\perp} = -\text{sgn}(I)\hat{\boldsymbol{p}}_{AB} \times \hat{\boldsymbol{k}} \tag{27}$$

These relative equations are solved using fsolve, a MATLAB® function, to determine the equilibrium configurations of x_A and y_A.

In the simulation results presented, we use an aluminum tether of 1-mm cross section. (See the Appendix for the aluminum properties.) Satellite $\mathcal{B}$ is assumed to be at an orbital radius $p_B = R_0 = 7671$ km. The total unstretched arc length of the tether is $L = 5$ km. The magnetic dipole strength is taken from International Geomagnetic Reference Field 2000 values.

Figure 3 shows the four equilibrium configurations, when $m_A = 100$ kg and $\text{Res}_u = 50\ \Omega$. The two equilibrium configurations along $\hat{\boldsymbol{e}}_r$ are nearly symmetric, and the two equilibrium configurations along $\hat{\boldsymbol{e}}_\theta$ are also nearly symmetric. For a rigid model of the tether, Mankala et al.[6] have shown that the tether has four similar relative equilibrium configurations. Of these four, the ones close to $\hat{\boldsymbol{e}}_r$ are stable and the ones close to $\hat{\boldsymbol{e}}_\theta$ are unstable. However, in the present model, a local eigenvalue analysis shows that all four configurations shown in Fig. 3 are unstable.

Figure 4a shows the relative equilibrium configurations of the tether (in quadrant 4) for different values of control resistance Res_u ranging from 0 to 300 Ω and m_A fixed at 30 kg. Similar symmetric configurations exist in quadrant 3. Observe that as the resistance in the circuit increases the equilibrium configuration gets close to the vertical and straighter. In the limit, when $\text{Res} \to \infty$, the tether is aligned along $\hat{\boldsymbol{e}}_r$, similar to a nonconductive tether. Figure 4b shows the relative equilibrium configurations of the tether (in quadrant 4) for different values of m_A ranging from 30 to 300 kg and Res_u fixed at 0 Ω. Similar symmetric configurations exist in quadrant 3. As mentioned earlier, the equilbrium configurations shown in Fig. 4 are unstable. A transient simulation of the system starting around the equilibrium configuration confirms it. Local eigenvalue analysis gives positive eigenvalues, showing that the equilibrium configurations are unstable. Beletsky and Levin[7] have noted that the charateristic equation of the locally perturbed system has positive roots. In their analysis, they assumed that the current is constant with respect to the perturbations in position of $\mathcal{A}$.

IV. Local Stabilization: Linear Control

For an inverted pendulum, it is possible to stabilize the system around the unstable vertical equilibrium by designing a controller based on the linearized model of the system around the equilibrium. As expected, this controller will have a certain domain of attraction when implemented on the actual nonlinear system. For the case of massless tether system, we design a similar controller to stabilize the system around the unstable equilibrium. When $\boldsymbol{Z} = [x_A, \dot{x}_A, y_A, \dot{y}_A]^T$ is defined, where $\boldsymbol{p}_{AB} = x_A\hat{\boldsymbol{e}}_r + y_A\hat{\boldsymbol{e}}_\theta$, the system dynamics can be expressed as

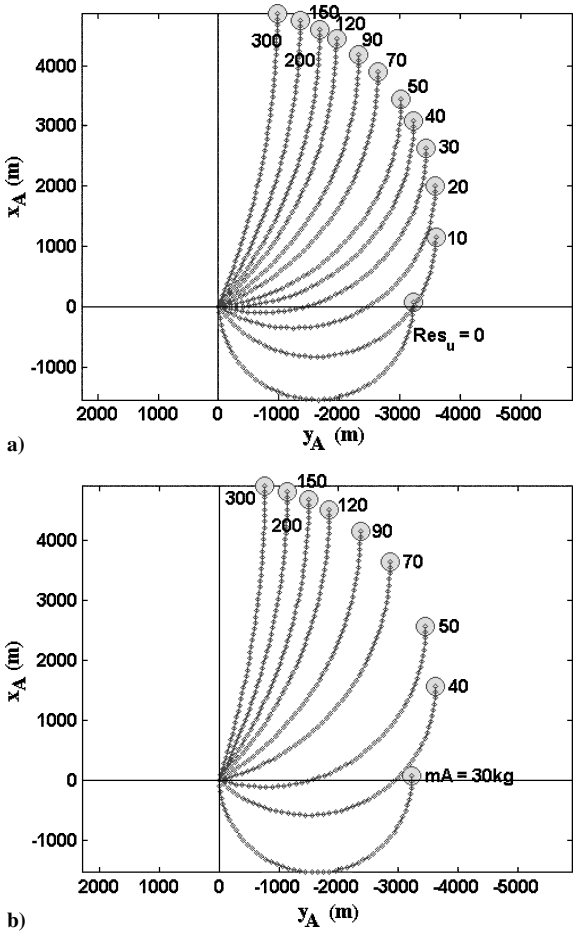

Fig. 4 Equilibrium configurations of massless tether system: a) for different values of Res_u with $m_A = 30$ kg and b) for different values of m_A when $\text{Res}_u = 0\ \Omega$.

$$\dot{\boldsymbol{Z}} = \boldsymbol{f}(\boldsymbol{Z}, \text{Res}) \tag{28}$$

Linearizing Eq. (28) around the equilibrium $\boldsymbol{Z}^*$ and Res^*, we get

$$\delta\dot{\boldsymbol{Z}} = A\delta\boldsymbol{Z} + b\delta\text{Res} \tag{29}$$

where

$$A = \left.\frac{\partial \boldsymbol{f}}{\partial \boldsymbol{Z}}\right|_{Z=Z^*,\ \text{Res}=\text{Res}^*}, \qquad b = \left.\frac{\partial \boldsymbol{f}}{\partial \text{Res}}\right|_{Z=Z^*,\ \text{Res}=\text{Res}^*}$$

It is found that, for any equilibrium configuration, two of the eigenvalues of A have nonnegative real parts, indicating that the equilibrium is unstable. However the linear system described by the A, b pair is found to be controllable for different equilibrium configurations. Thus, a linear state feedback controller, $\delta\,\text{Res} = -K\delta\boldsymbol{Z}$, can be used to place the poles of the closed-loop system $(A - bK)$ at desired locations in the left-half s plane. Because it is a four-state system, it is difficult to characterize the domain of attraction of this controller once it is applied to the nonlinear system. In the simulations, all of the poles of the closed-loop system were placed on the negative real axis to obtain a critically damped response. Also, choosing the poles close to the origin achieves slower speed of response. This allows the linear controller to have a larger domain of attraction when applied on the nonlinear system.

Figure 5 shows the effectiveness of the linear controller ($\text{Res} = \text{Res}^* + \delta\text{Res}$) when applied to the nonlinear system. The linear controller is chosen to stabilize the tether system around the equilibrium configuration corresponding to $\text{Res}_u = 50\ \Omega$ and $m_A = 30$ kg

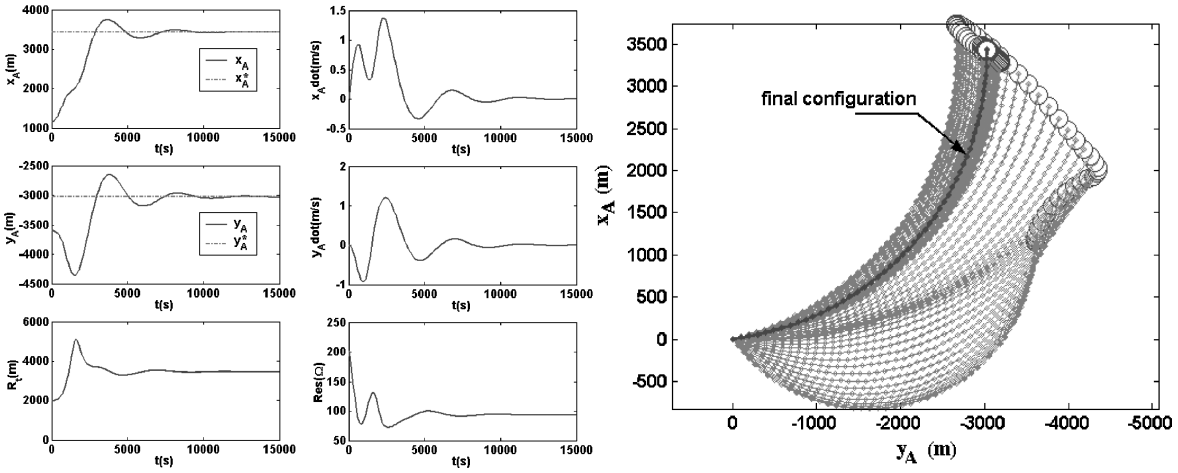

Fig. 5 Stabilization around $\text{Res}_u = 50\ \Omega$ with linear control.

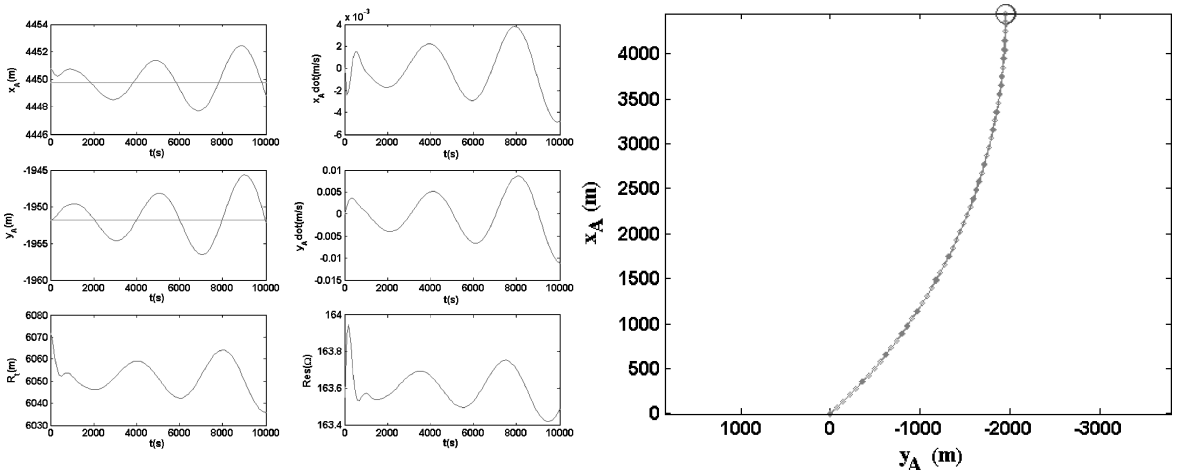

Fig. 6 Stabilization around $\text{Res}_u = 120\ \Omega$ with linear control.

(which corresponds to $x_A = 3434$ m and $y_A = -3026$ m). The poles for the closed-loop system were chosen as $[-2.5, -2.0, -1.5, -1.0] \times 10^{-3}$. The system is initially left in the equilibrium configuration corresponding to $\text{Res}_u = 10\ \Omega$ and $m_A = 30$ kg (which corresponds to $x_A = 1153$ m and $y_A = -3597$ m). Even though there is a large initial error, the controller stabilizes the tether system around the desired equilibrium configuration. Please note that the total resistance is always positive and is greater than the inherent tether resistance, which in this case is around 43 Ω. The positivity of the resistance was not considered while designing the control law. Also, the slow response of the sytem induced by placing the poles closer to the origin keeps the control effort, in this case δRes, small.

We expect that the domain of attraction of the controller will depend on the closed-loop poles. It was observed that if the poles are chosen far off from the origin, the domain of attraction where the linear controller can stabilize the tether system is much smaller. The domain of attraction also depends on the equilibrium configuration around which the linearization is done. Figure 6 shows that the linear controller designed based on same closed-loop poles is unable to stabilize the system around the equilibrium configuration corresponding to $\text{Res}_u = 120\ \Omega$ even when the initial error is very small (1 m in the $\hat{\boldsymbol{e}}_r$ direction). In general, we observed that the linear controller easily stabilizes configurations close to the $y = -x$ line, that is, the domain of attraction is large. Equilibrium configurations close to vertical are found to be difficult to stabilize using the linear controller. We expect that a proper choice of gains can help stabilize the system around any equilibrium configuration. Also, once the domain of attraction of the linear controller is characterized, gain scheduling can be used to perform equilibrium-to-equilibrium maneuvers.

V. Feedback Linearization: Nonlinear Control

In the preceding section, a linear controller was developed to stabilize the tether system around an equilibrium configuration. In this section, we develop a nonlinear controller for maneuvering from one equilibrium to another. Conceptually, the system under consideration is an underactuated system, with only one input Res and two output states x_A and y_A. Because the current in the tether is dominated by x_A, we feedback linearize x_A dynamics using the control input Res (to be precise Res_u) and treat the y_A dynamics as the internal dynamics. To avoid large control inputs, we use a reference trajectory in the feedback linearization of x_A dynamics. This way we can reduce the chances of Res of being negative. In Ref. 6, the positivity of the resistance is handled in a more analytical way.

The following scalar differential equations describe the dynamics of $\mathcal{A}$:

$$\ddot{x}_A = (R_0 + x_A)\omega^2 + 2\dot{y}_A\omega - \left[GM(R_0 + x_A)\big/R_A^3\right] - (R_t B|I|/m_A r_A)[x_A\cos(\alpha) - y_A\sin(\alpha)\text{sgn}(I)] \tag{30}$$

$$\ddot{y}_A = y_A\omega^2 - 2\dot{x}_A\omega - \left(GMy_A\big/R_A^3\right) - (R_t B|I|/m_A r_A)[y_A\cos(\alpha) + x_A\sin(\alpha)\text{sgn}(I)] \tag{31}$$

We choose the feedback linearized dynamics of x_A to be of the form

$$\ddot{x}_A = v = \ddot{x}_{Ad} - K_1(\dot{x}_A - \dot{x}_{Ad}) - K_2(x_A - x_{Ad}) \tag{32}$$

where x_{Ad} indicates the desired trajectory, which in equilibrium settles to x_A^*. To achieve this closed-loop dynamics, we

require

$$\text{abs}(I) = \frac{m_A r_A}{R_t B_0} \times \left[\frac{-v + (R_0 + x_A)w^2 + 2\dot{y}_A\omega - GM(R_0 + x_A)\big/R_A^3}{x_A \cos(\alpha) - y_A \sin(\alpha)\text{sgn}(I)} \right]$$

$$\Rightarrow |\text{Res}| = \frac{|\mathcal{E}| R_t B_0}{m_A R_A} \times \left[\frac{x_A \cos(\alpha) - y_A \sin(\alpha)\text{sgn}(I)}{-v + (R_0 + x_A)\omega^2 + 2\dot{y}_A\omega - GM(R_0 + x_A)\big/R_A^3} \right] \quad (33)$$

Note that in Eq. (33) we have parameters R_t, α, and sign (I) on the right-hand side, which depend on Res. Thus, ideally, we have to treat the equation as an implicit equation in Res and solve for it to get the control input at any instant. However, in the simulations we used the value of the Res from the previous iteration to find these parameters. With this choice of controller, the y_A dynamics becomes

$$\ddot{y}_A = y_A\omega^2 - 2\dot{x}_A\omega - \frac{GMy_A}{R_A^3} - \left[\frac{y_A \cos(\alpha) + x_A \sin(\alpha)\text{sgn}(I)}{x_A \cos(\alpha) - y_A \sin(\alpha)\text{sgn}(I)} \right] \times \left[-v + (R_0 + x_A)\omega^2 + 2\dot{y}_A\omega - \frac{GM(R_0 + x_A)}{R_A^3} \right] \quad (34)$$

If $I > 0$, we can define

$$\frac{y_A \cos(\alpha) + x_A \sin(\alpha)}{x_A \cos(\alpha) - y_A \sin(\alpha)} = \frac{\cos(\gamma - \alpha)}{\sin(\gamma - \alpha)} = \cot(\gamma - \alpha) = \cot(\eta) \quad (35)$$

where

$$\sin(\gamma) = x_A\big/\sqrt{x_A^2 + y_A^2}, \qquad \cos(\gamma) = y_A\big/\sqrt{x_A^2 + y_A^2} \quad (36)$$

With the earlier notation, we can simplify the internal dynamics expression as

$$\Rightarrow \ddot{y}_A + 2\omega\cot(\eta)\dot{y}_A + \left(GM\big/R_A^3 - w^2\right)y_A = -2\omega\dot{x}_A - \cot(\eta)\left\{-v + (R_0 + x_A)\left[\omega^2 - GM\big/R_A^3\right]\right\} \quad (37)$$

When $x_A \to x_{Ad} \to x_A^*$ and $\dot{x}_A = \ddot{x}_A = 0$, the internal dynamics becomes

$$\ddot{y}_A + \underbrace{2\omega\cot(\tilde{\eta})}_{c_1}\dot{y}_A + \underbrace{\left(GM\big/R_A^3 - w^2\right)}_{c_2}y_A + \underbrace{\cot(\tilde{\eta})\left(R_0 + x_A^*\right)\left[\omega^2 - GM\big/\tilde{R}_A^3\right]}_{c_3} = 0 \quad (38)$$

where $\cot(\tilde{\eta})$ and $\tilde{R}_A$ are obtained by replacing x_A with x_A^* in $\cot(\eta)$ and R_A, respectively. If the solution of Eq. (38) can be proved to be asymptotic or bounded stable, we can say that the nonlinear controller will always work. The response of the detailed internal dynamics depends on x_A^* and the value of y_A and $\dot{y}_A$ when x_A reaches its steady state x_A^*. Because it is difficult to prove analytically the stability of the preceding internal dynamics, we look at the phase plot of the system for different values of x_A^* with m_A fixed at 30 kg.

Figure 7 shows the phase plots for different values of x_A^*. In Fig. 7, the notation xA10 represents the phase plot corresponding to the equilibrium value (x_A^*) of x_A for $\text{Res}_u = 10\Omega$. In a phase plot, different phase trajectories are drawn for different initial states of y_A $(\dot{y}_A = 0)$ around y_A^*. The farthest initial state considered to find

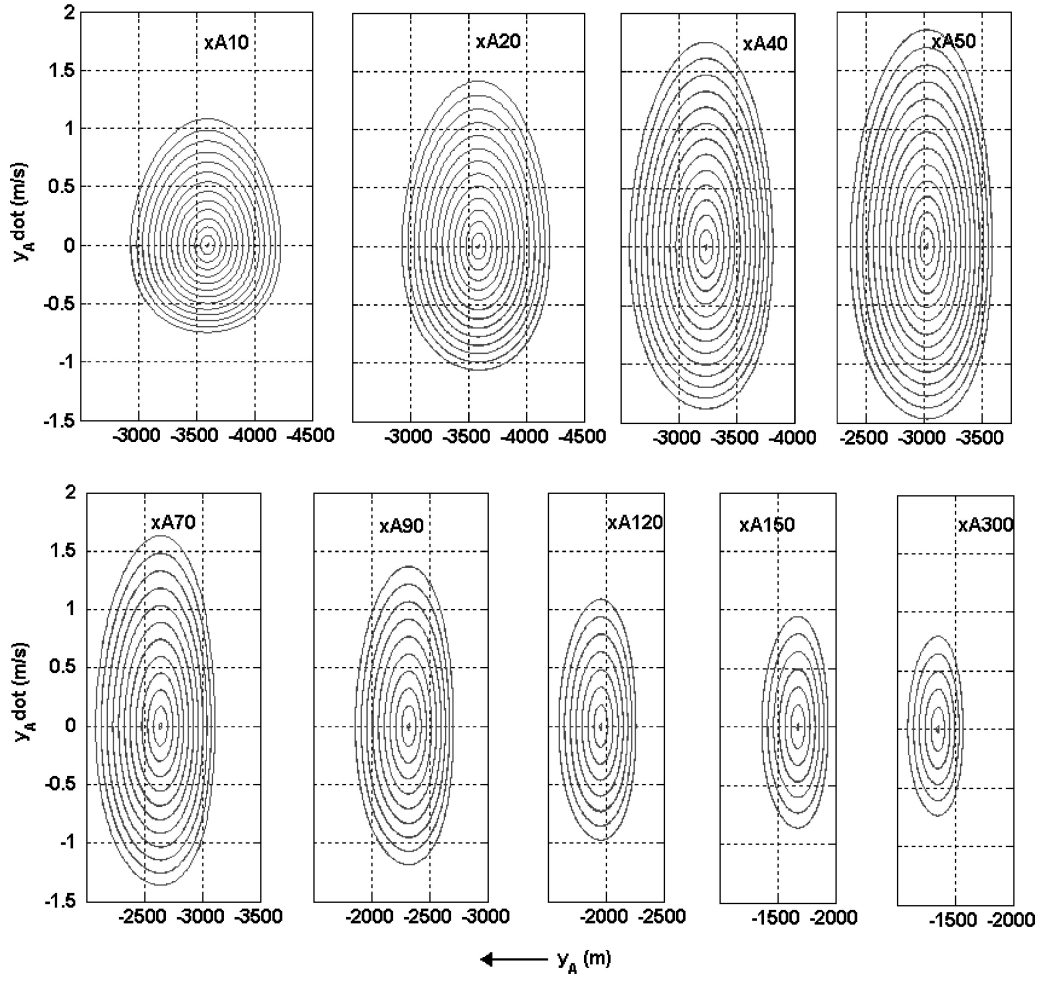

Fig. 7 Phase plots of internal dynamics for different values of x_A^*.

the phase trajectories is 660 m from y_A^*. If the phase trajectory is not stable beyond a particular initial state, it is not included in the phase plot. We see that in Fig. 7, the width of the stable periodic trjectories from xA10 to xA50 is the same indicating that they might have wider periodic trajectories. From xA70 onward, the width (on x axis) of the periodic trajectories continously reduces. To explain this trend for these equilibrium configurations, we can do the following: 1) Fix x_A at x_A^*, and 2) then perturb y_A from y_A^*. The minimum perturbation at which the tether becomes straight (singular configuration) is roughly related to the width of the stable periodic trajectories on the phase plot. For example, for xA90, this minimum perturbation at which tether is straight can be calculated as $y_A^* + \sqrt{(L^2 - x_A^{*2})} \approx 408$ m. From the Fig. 7 plot we can see that distance of the outermost trajectory from $(y_A^*, 0)$ measured along the decreasing y_A coordinate is also close to 400 m. This analysis indicates that the less is the curvature of the tether in the equilibrium configuration the less will be the width of the stable periodic trajectories in the internal dynamics phase plot. Because the electrodynamic forces act perpendicular to the tether, a straight (singular) configuration would require that the tension is infinite to balance the electrodynamic forces. Thus, this singular configuration acts as an infinite barrier in this model and, hence, does not permit the system to cross it unless due to numerical reasons during simulation. This can be the physical reason for the dependence of the regime of stable periodic trajectories on the distance to the singular configuration.

If the state $[y_A, \dot{y}_A]^T$ falls within this width when x_A dynamics reaches its steady state x_A^*, we can say that the y_A dynamics will be bounded stable. During the transient period, when x_A has not reached its steady state x_A^*, we can only show through simulations that the controller takes y_A close to y_A^*.

Figure 8 shows a simulation result when the already mentioned nonlinear controller is used to perform a maneuver from the equilibrium configuration correspoding to $\text{Res}_u = 10\ \Omega$ (in quadrant 3) to equilibrium configuration corresponding to $\text{Res}_u = 50\ \Omega$ (in quadrant 3). We see that x_A tracks x_{Ad}, which finally stabilizes around x_A^* correspoding to $\text{Res}_u = 50\ \Omega$. Internal dynamics y_A is bounded stable with peak-to-peak amplitude of y_A restricted to 35 m. The total time of maneuver is chosen to be 30,000 s. Figure 9 shows the simulation result for the same maneuver with total time of maneuver restricted to 12,000 s. Note that in this case also x_A stabilizes to x_A^* but the oscillations in y_A have increased (peak-to-peak amplitude of 1000 m). In relation to Fig. 7, we can say that when x_A stabilizes to x_A^*, the state $(y_A, \dot{y}_A)$ falls on a phase trajectory that is farther away from $(y_A^*, 0)$ than the one in the earlier simulation result. Hence, the amplitude of oscillation is greater in the second case. Figure 10 shows the simulation result when the nonlinear controller is used to perform a maneuver from the equilibrium configuration corresponding to $\text{Res}_u = 10\ \Omega$ (in quadrant 4) to the equilibrium configuration corresponding to $\text{Res}_u = 300\ \Omega$ (in quadrant 4). The total time of maneuver in this case is taken as 30,000 s. In this case, too, x_A stabilizes to x_A^*, but y_A oscillates about y_A^* with a peak-to-peak amplitude of 90 m. Note that in all of the simulations the total resistance Res is always positive and greater than Res_i. It was observed that this nonlinear controller failed to perform maneuvers from equilibrium

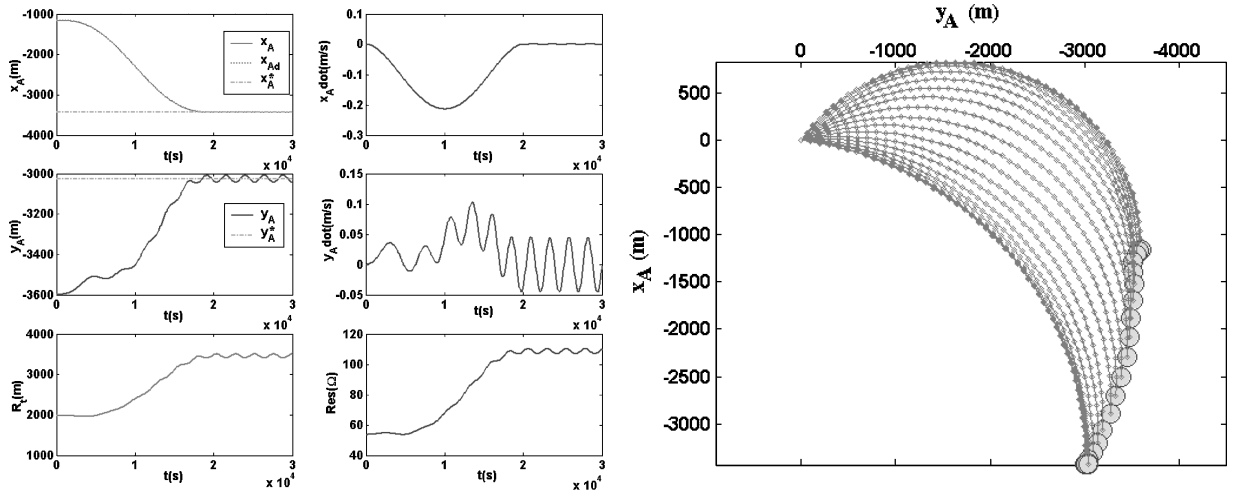

Fig. 8 Nonlinear controller: maneuver from $\text{Res}_u = 10\ \Omega$ equilibrium configuration to $\text{Res}_u = 50\ \Omega$ equilibrium configuration; total time of maneuver 30,000 s.

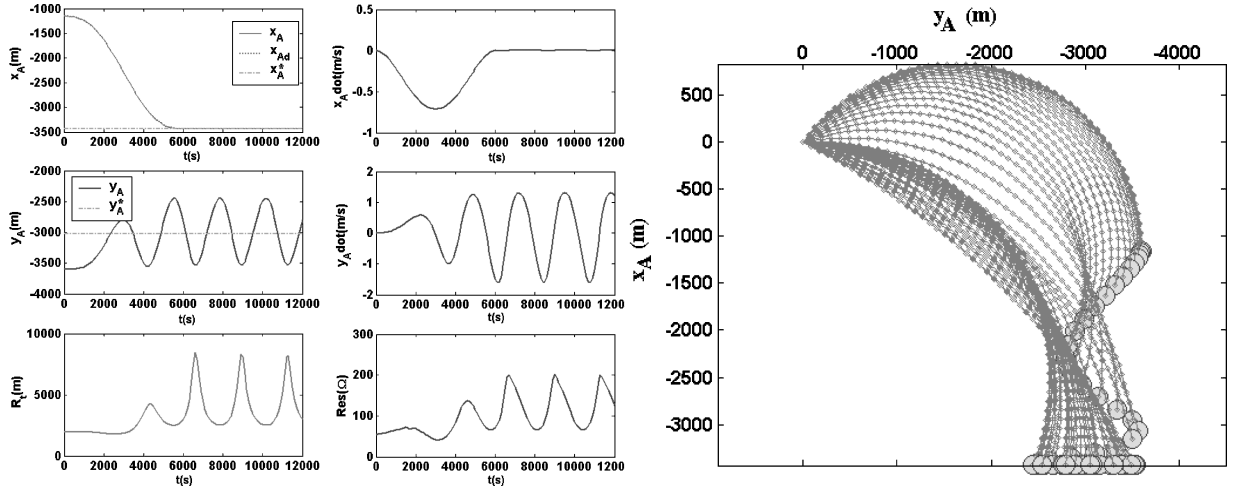

Fig. 9 Nonlinear controller: maneuver from $\text{Res}_u = 10\ \Omega$ equilibrium configuration to $\text{Res}_u = 50\ \Omega$ equilibrium configuration; total time of maneuver 12,000 s.

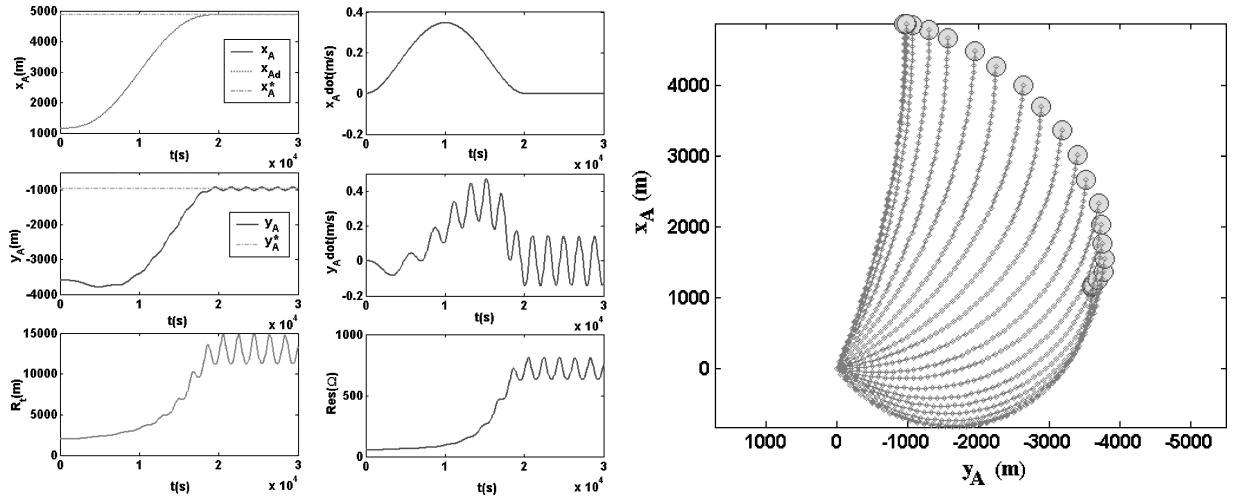

Fig. 10 Nonlinear controller: maneuver from $\text{Res}_u = 10\ \Omega$ equilibrium configuration to $\text{Res}_u = 300\ \Omega$ equilibrium configuration; total time of maneuver 30,000 s.

configurations in one quadrant to equilibrium configurations in the other, that is, maneuvers that span two quadrants.

A linear controller with a proper choice of gains can be used to reduce the steady-state oscillations of y_A induced by the nonlinear controller. This strategy is similar to the case of an inverted pendulum where 1) a Lyapunov controller is used to take the pendulum from stable equilibrium to the vicinity of the unstable equilibrium and 2) a linear controller based on the linearization of the system around unstable equilibrium is used to stabilize the pendulum around the unstable equilibrium.

VI. Conclusions

A massless tether system the main satellite of which is restricted to circular equatorial orbits is considered. With a nontitled dipople magnetic field and linear current law, we find the equilibrium configurations of the system. Because all of the equilibrium configurations are unstable, a stabilizing linear controller based on the linearization of the system around the equilibrium is developed. It was observed that the linear controller has a larger domain of attraction when the poles of the closed-loop system were placed closer to the origin. To do equilibrium-to-equilibrium maneuvers, we developed a nonlinear controller based on feedback linearization of x_A dynamics alone. The steady-state internal dynamics was found to have stable periodic trajectories around the equilibrium y_A^*. The amplitude of oscillation decreased with an increase in the time of maneuver because of lesser accelerations present in the system. The nonlinear controller was found to be ineffective for maneuvers that span two (third and fourth) quadrants. A linear controller in conjuction with nonlinear controller may give desirable behavior. In both the controllers, the total resistance Res was always positive and greater than the inherent tether resistance Res_i indicating that the control resistance Res_u is always positive. Finally, the controllers developed are valid from the current I law perspective even in the case when the current collection and emf E generated are not linearly related. The only limitation is to make sure that the maximum current required by the controllers is within the maximum current collection possible through plasma contactors. Rather, only those maneuvers are possible for which the current requirement is less than that of the maximum possible current collection.

Appendix: Tether Material Properties

The properties of aluminum tether used in the simulations are density $= 2700\ \text{kg/m}^3$, specific conductivity $= 27.4 \times 10^{-9}\ \Omega\text{m}$, Young's modulus $= 70 \times 10^9$ Pa, and inherent resistance = (specific conductivity $\times$ L/area of cross section).

References

[1]Forward, R. L., Hoyt, R. P., and Uphoff, C. W., "Terminator Tether: A Spacecraft Deorbit Device," *Journal of Spacecraft and Rockets*, Vol. 37, No. 2, 2000, pp. 187–196.

[2]Vannaroni, G., Dobrowolny, M., and De Venuto, F., "Deorbiting with Electrodynamic Tethers: Comparison Between Different Tether Configurations," *Space Debris*, Vol. 1, 2001, pp. 159–172.

[3]Irwin, E. V., Thomas, J. K., and Ethan, A. S., "Space Station Reboost with Electrodynamic Tethers," *Journal of Spacecraft and Rockets*, Vol. 37, No. 2, 2000, pp. 154–164.

[4]Estes, R. D., Sanmartn, J., and Martnez-Suchez, M., "Performance of Bare-Tether Systems Under Varying Magnetic and Plasma Conditions," *Journal of Spacecraft and Rockets*, Vol. 37, No. 2, 2000, pp. 197–204.

[5]Mankala, K. K., Agrawal, S. K., "Dynamic Modeling and Simulation of Impact in Tether Net/Gripper Systems," *Multibody System Dynamics*, Vol. 11, No. 3, 2004, pp. 235–250.

[6]Mankala, K. K., and Agrawal, S. K., "Equilibrium-to-Equilibrium Maneuvers of Rigid Electrodynamic Tethers," *Journal of Guidance, Control, and Dynamics*, Vol. 28, No. 3, 2005, pp. 541–545.

[7]Beletsky, V. V., and Levin, E. M., *Dynamics of Space Tether Systems*, American Astronautical Society, San Diego, CA, 1993, Chap. 5.

[8]Corsi, J., and Iess, L., "Stability and Control of Electrodynamic Tether for Deorbiting Applications," *Acta Astronautica*, Vol. 48, No. 5–12, 2001, pp. 491–501.

[9]Pelaez, J., Lorenzini, E. C., Ruiz, M., and Lopez-Rebollal, O., "A New Kind of Dynamic Instability in Electrodynamic Tethers," *Journal of Astronautical Sciences*, Vol. 48, No. 4, 2000, pp. 449–476.

[10]Dobrowolny, M., "Lateral Oscillations of an Electrodynamic Tether," *Journal of Astronautical Sciences*, Vol. 50, No. 2, 2002, pp. 125–147.

[11]Mankala, K. K., and Agrawal, S. K., "Dynamic Modeling and Simulation of Satellite Tethered Systems," *Journal of Vibration and Acoustics*, Vol. 127, No. 2, 2005, pp. 144–156.

[12]Resnick, R., and Halliday, D., *Physics*, Wiley, New York, 1978.

I. Vas
Associate Editor